Acta Oceanol. Sin., 2016, Vol. 35, No. 3, P. 90–101
DOI: 10.1007/s13131-016-0820-2
http://www.hyxb.org.cn
E-mail: hyxbe@263.net

Assessment of intraseasonal variabilities in China Ocean Reanalysis (CORA)

ZHANG Min[1], ZHOU Lei[2]*, FU Hongli[3], JIANG Lianghong[2], ZHANG Xiangming[2]

[1] Key Laboratory of Coastal Disaster and Defence of Ministry of Education, Hohai University, Nanjing 210098, China

[2] State Key Laboratory of Satellite Ocean Environment Dynamics, Second Institute of Oceanography, State Oceanic Administration, Hangzhou 310012, China

[3] Key Laboratory of Marine Environment Information Technology, National Marine Data and Information Service, State Oceanic Administration, Tianjin 300171, China

Received 1 June 2015; accepted 13 November 2015

Abstract

A regional reanalysis product—China Ocean Reanalysis (CORA)—has been developed for the China's seas and the adjacent areas. In this study, the intraseasonal variabilities (ISVs) in CORA are assessed by comparing with observations and two other reanalysis products (ECCO2 and SODA). CORA shows a better performance in capturing the intraseasonal sea surface temperatures (SSTs) and the intraseasonal sea surface heights (SSHs) than ECCO2 and SODA do, probably due to its high resolution, stronger response to the intraseasonal forcing in the atmosphere (especially the Madden-Julian Oscillation), and more available regional data for assimilation. But at the subsurface, the ISVs in CORA are likely to be weaker than reality, which is probably attributed to rare observational data for assimilation and weak diapycnal eddy diffusivity in the CORA model. According to the comparison results, CORA is a good choice for the study related to variabilities at the surface, but cares have to be taken for the study focusing on the subsurface processes.

Key words: China Ocean Reanalysis (CORA), intraseasonal variability, Madden-Julian Oscillation, ocean reanalysis product

Citation: Zhang Min, Zhou Lei, Fu Hongli, Jiang Lianghong, Zhang Xiangming. 2016. Assessment of intraseasonal variabilities in China Ocean Reanalysis (CORA). Acta Oceanologica Sinica, 35(3): 90–101, doi: 10.1007/s13131-016-0820-2

1 Introduction

Ocean reanalysis products, which combine the ocean model and observations from different sources using the data assimilation technique, have become a very important data source for almost all research fields in oceanography. So far, a few global ocean reanalysis products have been generated and broadly utilized, such as the Estimating the Circulation and Climate of the Ocean (ECCO; Stammer and Chassignet, 2000; Wunsch and Stammer, 2003) and the Simple Ocean Data Assimilation (SODA; Carton and Giese, 2008; Carton et al., 2000a, b). However, the oceanic processes and the structure of marginal seas, such as the China's seas, are affected not only by changes of the global oceanic environment, but also significantly affected by the local environment (Han et al., 2011). Thus, a regional ocean reanalysis product focusing on the China coastal waters and adjacent seas, named as the China Ocean Reanalysis (CORA), was proposed and generated a few years ago by the National Marine Data and Information Service (Han et al., 2011, 2013b).

Many studies have been conducted to evaluate the capability of CORA. For the global version of CORA, the climatology temperature in the upper ocean has a comparable quality with SODA, except for the areas around 40°S, and the CORA temperature errors are noticeably smaller than those in SODA in the deep ocean due to the strong subsurface data constraints in CORA (Han et al., 2013a). On interannual time scales, El Niño-Southern Oscillation (ENSO) is the dominant process. The global version of CORA is able to reproduce major ENSO events (Han et al., 2013a). Regionally, the responses to ENSO in the South China Sea (SCS) are also more realistic than SODA, as shown with the correlations between the interannual SSTs and the ENSO index (Wu, 2012; Wu et al., 2013). On the seasonal time scale, the mean seasonal variation in the upper ocean heat content (OHC) in CORA is similar to the one in the World Ocean Atlas 2009 (Han et al., 2013a).The fingerprints of Asian monsoon are well captured by CORA (Wu et al., 2013). Specifically, there is a large cold eddy off the coast of Vietnam in summer; there are large zonal temperature gradients between the Luzon cold eddy and the warm Kuroshio; and the isotherms at the surface are nearly parallel to the latitude in the northern SCS in both summer and winter. All these distinct features are clearly reproduced in CORA (Wu, 2012).

Previous studies mainly focused on time scales longer than a season. Actually, the variabilities on intraseasonal time scales, which have periods between 30 and 60 days, are also energetic components over the China's seas. The ratios between the variance of intraseasonal variabilities (ISVs) and the variance of total

Foundation item: The National Natural Science Foundation of China under contract Nos 41206178, 41376034, 41276018 and 41321004; the Fundamental Research Funds for the Central Universities under contract No. 2014B30514; the open project supplied by the Key Laboratory of Marine Environmental Information Technology, National Marine Data and Information Service, State Oceanic Administration: Effectiveness on the intraseasonal scale in CORA (2015–2016); the Predictability of Ocean Dynamical System Project under Contract No. 151053.
*Corresponding author, E-mail: lzhou@sio.org.cn

variabilities in SSHs and SSTs are shown in Fig. 1a and Fig. 1b. The ISVs are obtained with a band-pass filtering between 20 days and 100 days, which are common cut-off periods for isolating ISVs. Two examples of the power spectra (one for SSH and one for SST) are shown in Figs 1c and d. In most regions in the SCS, the ISVs account for more than 20% of the total variance. In some specific regions, such as the intraseasonal SSHs around the Luzon Strait and the Vietnam coast, the ISVs can account for more than 50%. Over the western Pacific, the intraseasonal SSHs take up to around 50% of the total variance in a zonal region centered around 20°N, while the intraseasonal SSTs take up to 40% of the total variance around the equator. There are large ratios for the intraseasonal SSHs in the East China Sea, which, however, may be caused by the errors of altimeter data in shallow waters (Ponte et al., 2007). In Figs 1a and b, it seems that there is a latitude-dependent distribution of pronounced ISVs, as studied in Qiao et al. (2004), Zhai (2008) and Lin et al. (2014). Actually, if the domain is extended to the whole Pacific Ocean, the seeming zonal distribution does not exist. However, this does not indicate a contradiction to previous results, since the ISVs in this study are not decomposed into finer frequency bands, as did in the previous studies. Since the detection of ISVs requires high sampling frequency, very few *in situ* observations were capable of isolating the ISVs over the China's seas. Zhou et al. (1995) extracted the intraseasonal SSTs in the SCS from the hydro-meteorological data during the summer of 1985. With mooring data in the SCS, Zhou and Gao (2002) found ISVs with an amplitude of 1–2°C in the subsurface temperature from 50 m to 100 m depth. In addition, the oceanic ISVs in the SCS are found to be closely related to the Madden-Julian Oscillation (MJO), which is the major ISV component in the atmosphere (Madden and Julian, 1971; Zhang, 2005; Kajikawa et al., 2009). Wang et al. (2013) pointed out that the MJO is important for summer ocean circulation and temperature in the SCS. MJO can enhance the cyclonic (anticyclonic) circulation by producing a positive (negative) wind stress curl in the northern (southern) SCS during its westerly phase. And MJO

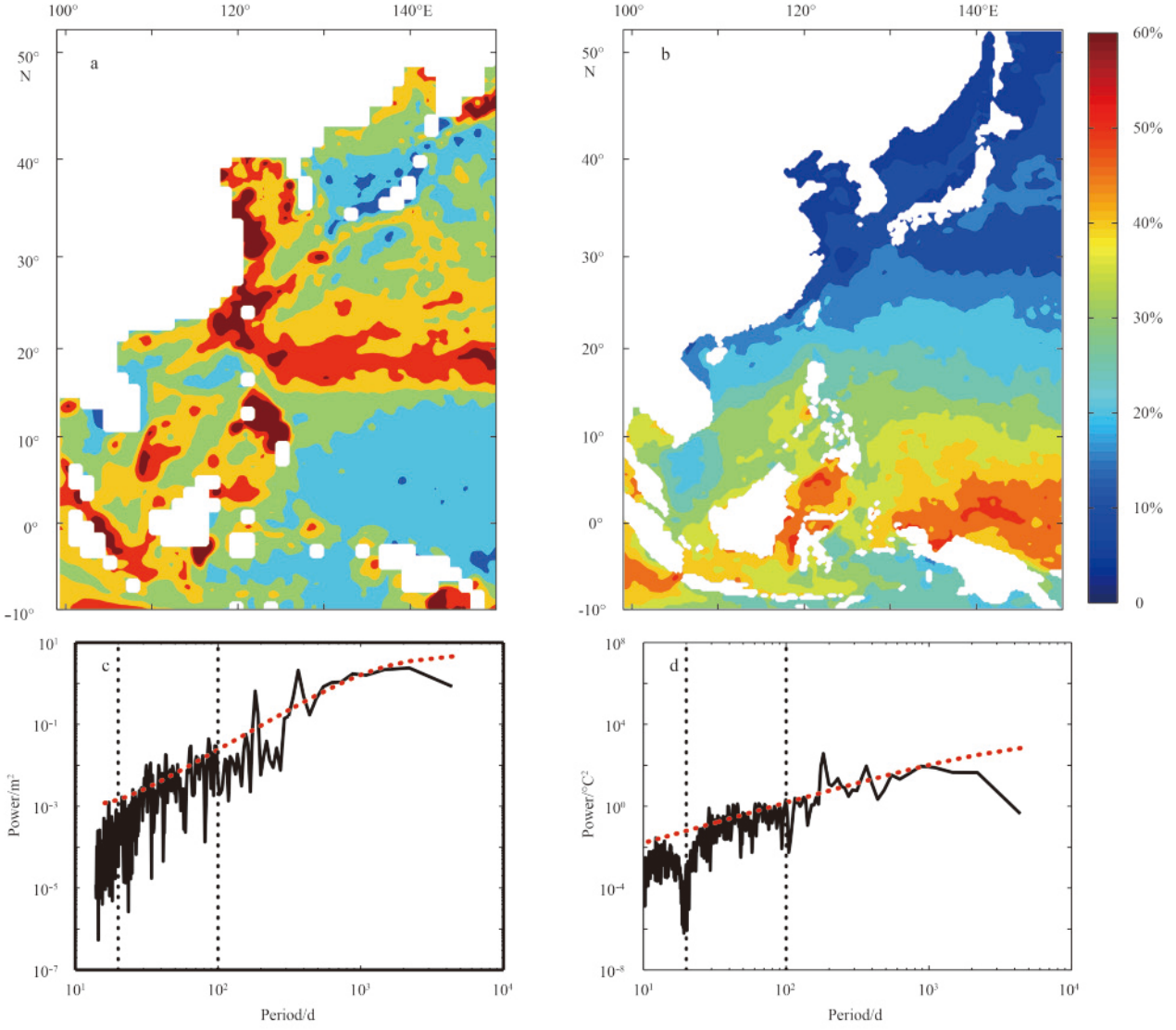

Fig. 1. Ratios between the variance of ISVs and the total variance of SSHs (a). Figure 1b is the same as Fig. 1a but for SSTs. Power spectra of SSH (c) and SST (d) in the region from 10°S to 10°N and from 99°E to 130°E, where the ISVs are strong, are shown with black lines. The red dashed lines show the reference spectra using the auto-regression at a significance level of 95%. The vertical black dash lines mark the cutoff periods at 20 d and 100 d.

has a reversed but weaker effect on the ocean circulation and temperature in SCS during its easterly phase (Li et al., 2014). Since the ISVs are non-negligible over the China's seas, it is necessary to have a comprehensive evaluation on the ability of the CORA to capture the oceanic ISVs and this is the motivation of this study.

In this study, the ISVs in CORA are assessed against observations and two other widely-used global reanalysis products, which are introduced in Section 2. The ISVs in SSH and SST are compared in Section 3 and the ISVs in the subsurface processes are compared in Section 4. Then, the conclusions and discussion are presented in Section 5.

2 Data and method

The model domain for CORA is from 10°S to 52°N and from 99°E to 148°E, which covers all coastal China's seas (the Bohai Bay, the Yellow Sea, the East China Sea, the South China Sea) and the adjacent seas. CORA yields daily mean outputs with 35 vertical levels. The horizontal resolution changes with locations, as shown in Fig. 2. The finest horizontal resolution is (1/8)° latitude ×(1/8)° longitude in the East China Sea, over the Kuroshio region, and around Taiwan. The coarsest horizontal resolution is (1/2)° latitude ×(1/2)° longitude in the four corners of the model domain (Fig. 2). The CORA product starts from 1958 and lasts until 2011. Now, the version 1 CORA dataset can be downloaded from the CMOC China website (http://www.cmoc-china.cn). The CORA reanalysis product adopts the Princeton Ocean Model with a generalized coordinate system (POMgcs; Mellor et al., 2002; Ezer and Mellor, 2004), and assimilates the observations using a sequential three-dimensional variational (3D-Var) scheme (Li et al., 2008; Li, 2008).

The SSTs are obtained from the daily Optimal Interpolation SST Analysis (version 2; OISST2; Reynolds et al., 2007) with a horizontal resolution of (1/4)° latitude × (1/4)° longitude, provided by National Oceanic and Atmospheric Administration (NOAA). The SSHs are obtained from the Delayed Time (DT) Reference (Ref) merged weekly gridded sea level data with a resolution of (1/3)° latitude × (1/3)° longitude, provided by the Data Unification and Altimeter Combination System (DUACS) and distributed by Archiving, Validation, and Interpretation of Satellite Data in Oceanography (AVISO). The SSH data has already been corrected for the instrument error and the corresponding geophysical factors. The hourly ocean velocities in the northern Ombai Strait and the Lombok Strait are obtained from the International Nusantara Stratification and Transport (INSTANT) program. The data last from August 2003 to the end of 2006 (Sprintall et al., 2004).

Besides the analysis data and merged products, CORA is also compared with two global reanalysis products, SODA (version 2.1.6; Carton and Giese, 2008) and ECCO2 (Menemenlis et al., 2008). SODA has a time resolution of 5 days, a horizontal spatial resolution of (1/2)° latitude × (1/2)° longitude, and 40 layers in the vertical. ECCO2 was established as part of the World Ocean Circulation Experiment (WOCE) with the goal of combining a general circulation model (GCM) and various observations, in order to produce a quantitative depiction of the time-evolving global ocean state (Menemenlis et al., 2008). Since the temperature of ECCO2 is not supplied, the upper ocean temperature is calculated with the potential temperature, density, surface pressure, and sea water pressures per UNESCO 1983 report (Fofonoff and Millard, 1983). ECCO2 has a horizontal resolution of (1/4)° latitude × (1/4)° longitude and 50 vertical layers. The temporal resolutions for SST and SSH in ECCO2 are daily, while they are 3 days for the three-dimensional ocean temperature and ocean current.

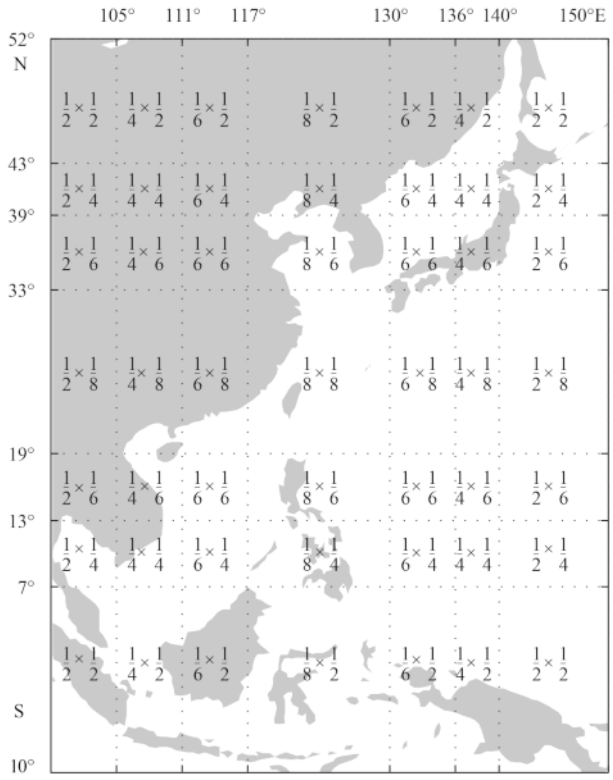

Fig. 2. Spatial resolutions in the CORA domain. The numbers in each box denote the horizontal resolution. For example, 1/8 × 1/6 denotes a resolution of (1/8)° latitude × (1/6)° longitude.

Different data sets have different time spans. The altimeter data have the latest starting time in October, 1992 and SODA has the earliest ending time in December, 2008. Thus, the common period for all above data sets is from 1993 to 2007 and this period is selected for the following comparisons. The intraseasonal signals in this study are obtained with a butterworth band-pass filter. The cut-off periods are 20 days and 100 days (Figs 1c and d). All observations and reanalysis products are interpolated onto the CORA grids, which facilitates the point-to-point comparisons.

Since the ocean ISVs are closely related to the atmosphere ISVs, especially to the MJO. The daily index created by Wheeler and Hendon (2004) is utilized to represent the MJO. To accommodate SODA with a 5-day resolution, a new 5-day MJO index is calculated by taking the average of the daily MJO index within every 5 days specified in SODA. Correspondingly, the amplitude and phase of the 5-day MJO index are generated following Wheeler and Hendon (2004). A new 3-day MJO index is calculated similarly, in order to accommodate the three-dimensional variables in ECCO2 which have a 3-day resolution.

3 Calibrations on intraseasonal SSTs and intraseasonal SSHs

3.1 *Intraseasonal variabilities in SSTs and SSHs*

Since there are reliable satellite observations of SST and SSH, they are the focus of the following comparisons.

The standard deviations (STDs) of the intraseasonal SSHs and the intraseasonal SSTs (which are obtained with a band-pass filtering between 20 days and 100 days) are compared in Figs 3 and

Fig. 4, respectively. The largest ISVs in both SSHs and SSTs reside in the Kuroshio extension (Figs 3b and 4b), which are captured by CORA. In contrast, the ISVs over the Kuroshio extension are much stronger than reality in ECCO2, but are too weak in SODA. The ISVs are pronounced over the north Pacific bifurcation zone centered around 20°N, due to both local oceanic instabilities (Zhang et al., 2001) and intrusion eddies from the subtropical Pacific (Kobashi and Kawamura, 2001; Qiao et al., 2004). Such ISVs are captured in CORA and ECCO2, but the amplitudes are a little weaker than observations in ECCO2. The mean variances between 120°E and 130°E along 20°N are 0.07 m for T/P observations and CORA, but are 0.06 m for ECCO2. SODA hardly show the ISVs in this region, which is probably attributable to its low resolution. In the eastern China's seas, there are huge ISVs in the altimeter data, which are not resolved in any of the reanalysis products. Since the altimeter data tend to have large errors near the coast, these variabilities are doubtful (Ponte et al., 2007). For SSTs, there are pronounced ISVs in the East China Sea, the Yellow Sea, and the SCS. The most intense variabilities occur in the northeastern East China Sea and the southern Yellow Sea (Zeng et al., 2006; Zhou and Gao, 2002; Zhou et al., 1995). Such ISVs in SSTs are captured in CORA, but not in ECCO2 and SODA. As a regional reanalysis product focusing on the China's seas, more observations including the *in situ* data from shipboard instruments and buoys in the coastal China's seas are assimilated and hence a better performance of CORA than the global reanalysis is understandable. In the SCS, large ISVs in SSH exist in the northern part and off the Vietnam coast. In the former region, the ISVs are attributable to the internal variabilities from the Luzon Strait and corresponding oceanic instabilities (Wu and Chiang, 2007; Yang et al., 2014a, b), while in the latter region, the ISVs are associated with the upwelling and the jet current off Vietnam (Xie et al., 2003, 2007). These variabilities are reproduced in CORA and ECCO2, but the signals in ECCO2 seem too strong. The relation between the internal variabilities and ocean ISVs was studied previously, for example, over the tropical western Pacific Ocean

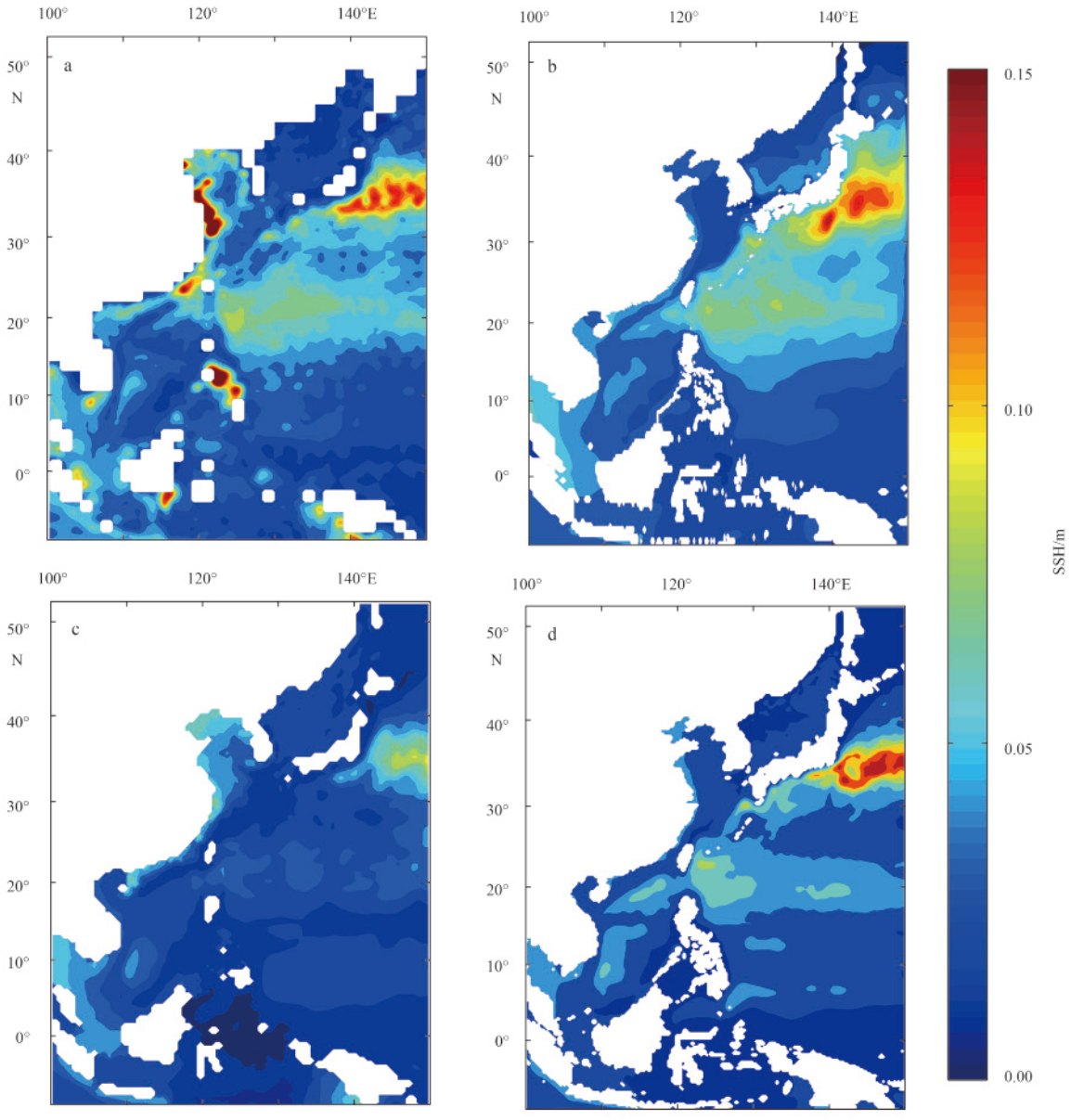

Fig. 3. The standard deviation of the intraseasonal SSH in observations (a), CORA (b), SODA (c), and ECCO2 (d).

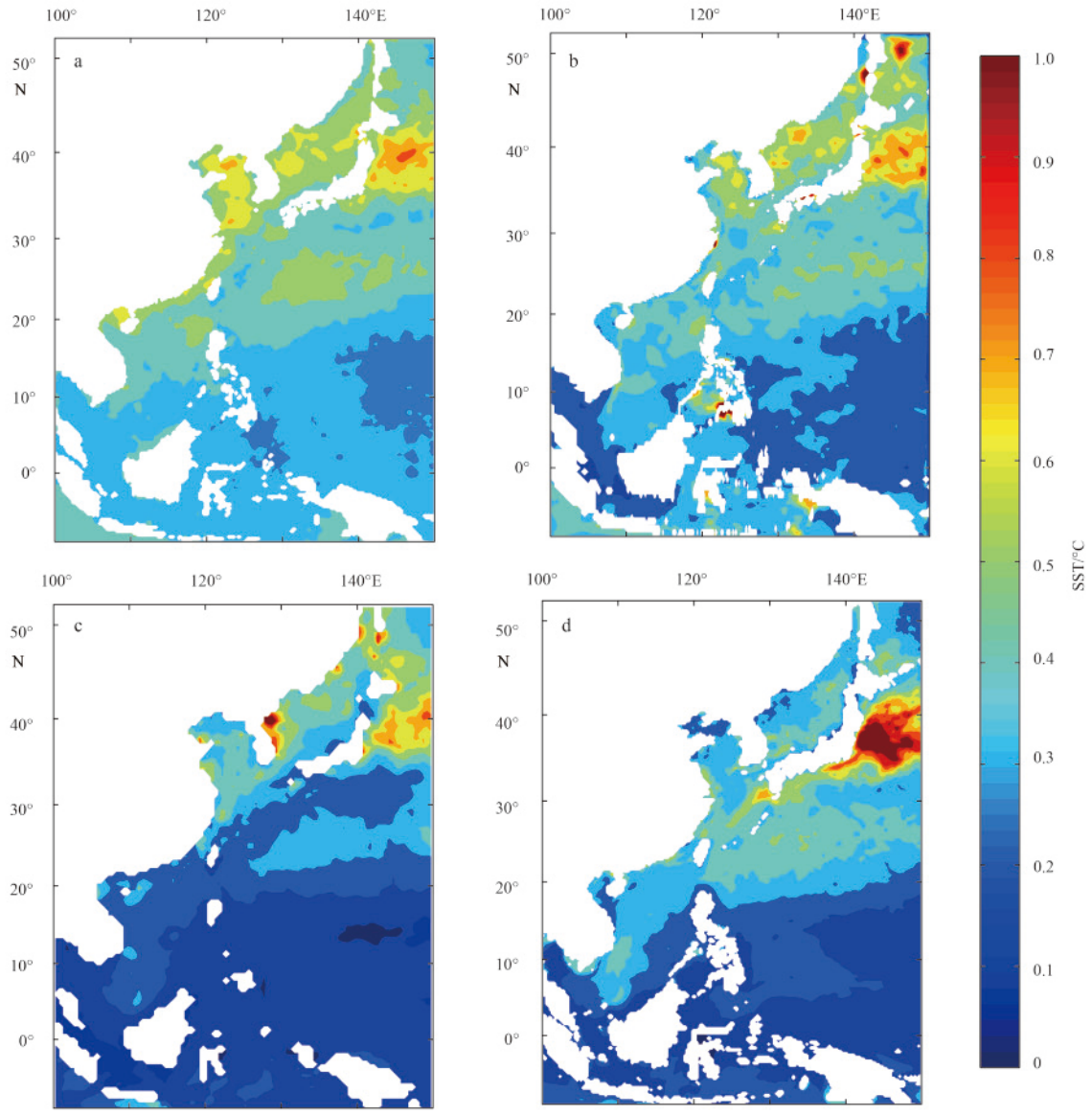

Fig. 4. The standard deviation of the intraseasonal SST in observations (a), CORA (b), SODA (c), and ECCO2 (d).

by Matthews et al. (2007), over the eastern Indian Ocean by Zhou and Murtugudde (2010), and over the western Indian Ocean by Zhou et al. (2008). However, over the CORA domain, intense studies on the mechanism of ocean ISVs are still required. SODA shows a moderate capability off Vietnam, but almost no signals in the northern SCS. The ISVs in SSTs are distinguished to the west of the Luzon Strait, which is only resolved in CORA but not in the other two global reanalyses. Over most SCS, the ISVs in SSTs are about 0.4°C. CORA yields the intraseasonal SSTs with similar amplitude but over a small region. In contrast, ECCO2 only captures the intraseasonal SSTs along the Vietnam coast and SODA have almost no ability to reproduce the intraseasonal SSTs.

3.2 *Composite intraseasonal SSTs at the MJO phases*

As the major component of the ISVs in the atmosphere, the MJO leaves clear footprints from the tropical to the subtropical oceans. Thus, it is necessary to calibrate the oceanic responses to the MJO forcing in CORA. As introduced above, the MJO is represented with the Real-time Multivariate MJO series 1 (RMM1), and RMM2 index created by Wheeler and Hendon (2004). The correlation coefficients (statistically significant at a 99% confidence level) between the intraseasonal SSTs from different data sets and RMM1/RMM2 are presented in Fig. 5. When RMM1 is positive, the deep convection center for MJO locates in the maritime continent. Heavy clouds due to convection reduce the shortwave radiation and the SSTs decrease accordingly. Thus, negative correlations are expected (Fig. 5a). CORA overestimates such negative correlations (Fig. 5b), while SODA (Fig. 5c) and ECCO2 (Fig. 5d) hardly reproduce the oceanic response to the convection during the MJO. Meanwhile, to the north of the MJO convection center, SSTs increase due to the high solar radiation in the clear sky. Hence, positive correlations are found between 10°N and 30°N, which is well reproduced in CORA. ECCO2 show some abilities to capture these positive correlations, but the regions are much wider than the observations. After a quarter phase of the MJO when the convection center moves to the western Pacific Ocean, RMM2 becomes positive and RMM1 turns al-

most zero, since these two components are in a quadrature relation. As a result, cumulus clouds reduce SSTs over the western Pacific Ocean and result in negative correlations between intraseasonal SSTs and RMM2 (Fig. 5e), which is captured, but overestimated, in all three reanalysis products (Fig. 5g–h).

For a detailed comparison, the composite intraseasonal SSTs in various data sets at the 8 MJO phases, which are defined with RMM1 and RMM2 (Wheeler and Hendon, 2004), are shown from Fig. 6 to Fig. 8. At Phase 1 when the MJO convection center is over the western hemisphere and far from the CORA domain, the intraseasonal SST components are moderate. From Phases 2 to 5 when the convection center travels from the Indian Ocean to the maritime continent, intraseasonal SST drops along the path due to the cloud-radiation feedback. Meanwhile, the clear sky to the north of the convection leads to positive SST anomalies, which extend northeastward from the SCS to the northwestern Pacific Ocean. While the convection center keeps moving eastward, at Phases 6 and 7, negative SST anomalies occur over the western Pacific Ocean and the oceanic responses reach the maximum. Since the MJO has a clear seasonality that it is stronger in boreal winter, the composite MJO forcing shifts to the northern hemisphere (not shown). Correspondingly, the oceanic responses can spread around 30°N. At Phase 8, the MJO convection usually diminishes after passing the international dateline and travels back to the western hemisphere. A clear sky is left behind, hence positive SST anomalies are seen from the maritime continent to the tropical Pacific. However, the negative SST anomalies over the SCS and the northwestern Pacific Ocean remains.

For CORA (Fig. 7), generally speaking, the patterns of the oceanic response to the MJO are similar to the observations, but the amplitudes are stronger than observations. For example, the negative SST anomalies from the maritime continent and the tropical Pacific from Phase 5 to Phase 7 are captured, but are overestimated in CORA. Over the SCS, the warm SST anomalies from Phase 3 to Phase 5 and the cold anomalies from Phase 7 to Phase 8 are reproduced well. Based on such evidences, one can surmise that sea surface response to the MJO is too strong, which is possibly attributed to weak diapycnal eddy diffusivity and uncoupled ocean-atmosphere flux terms in the CORA model. This will be implied again below, when making comparisons at the subsurface. Nevertheless, the process analysis is not the focus of this study. Thus, the in-depth diagnostics on the model mechanisms are not presented here, but will postponed to further study. In ECCO2, the composite SST anomalies are not so well reproduced (Fig. 8). The negative SST anomalies over the maritime continent due to cumulus clouds are missing. The warm anomalies over the SCS from Phase 3 to Phase 5 are discernable, but are too weak compared with observations. The negative SST anomalies at Phase 7 are confined to the south of 10°N, rather than extending to the northwestern Pacific Ocean as they are in reality. The composite intraseasonal SSTs at the MJO Phases in SODA are even less satisfactory (not shown).

4 Comparisons of the subsurface properties

Besides the ISVs in SSHs and SSTs, there are also pronounced ISVs at the subsurface (Wang et al., 2013; Zhou et al., 1995). However, there are no satellite observations at the subsurface to facilitate the calibration of CORA. Argo floats are a useful instrument to make measurements at the subsurface. However, until now, most gridded Argo products are monthly mean data, which cannot resolve ISVs. At any specific location, Argo profile data only last for tens of days, which are too short to isolate the ISVs. For a few other *in situ* observation projects, such as the Global Drifter Program and the Joint Archive for Shipboard ADCP, the data were not long enough to isolate the ISVs, either. The Kuroshio Extension Observations (KEO) yielded long enough

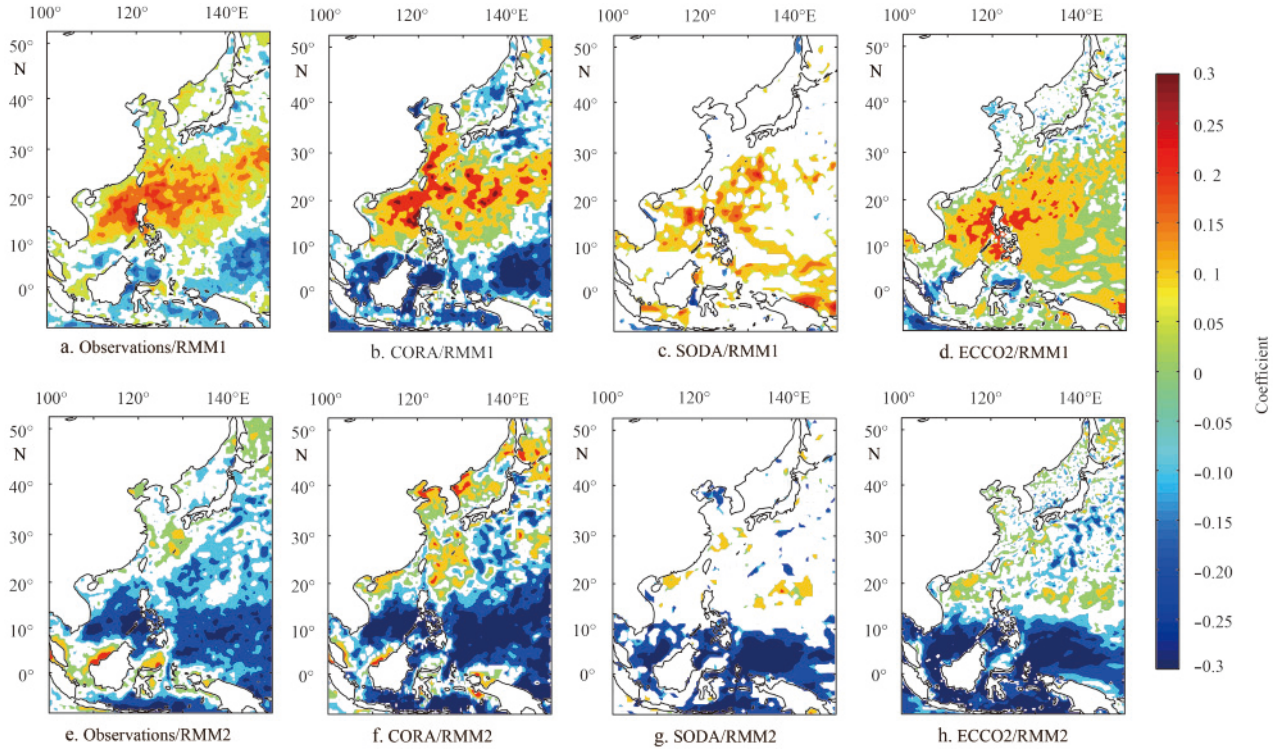

Fig. 5. Correlation coefficients between the intraseasonal SST and the MJO index. Only the coefficients that are statistically significant at a 99% confidence level are shown.

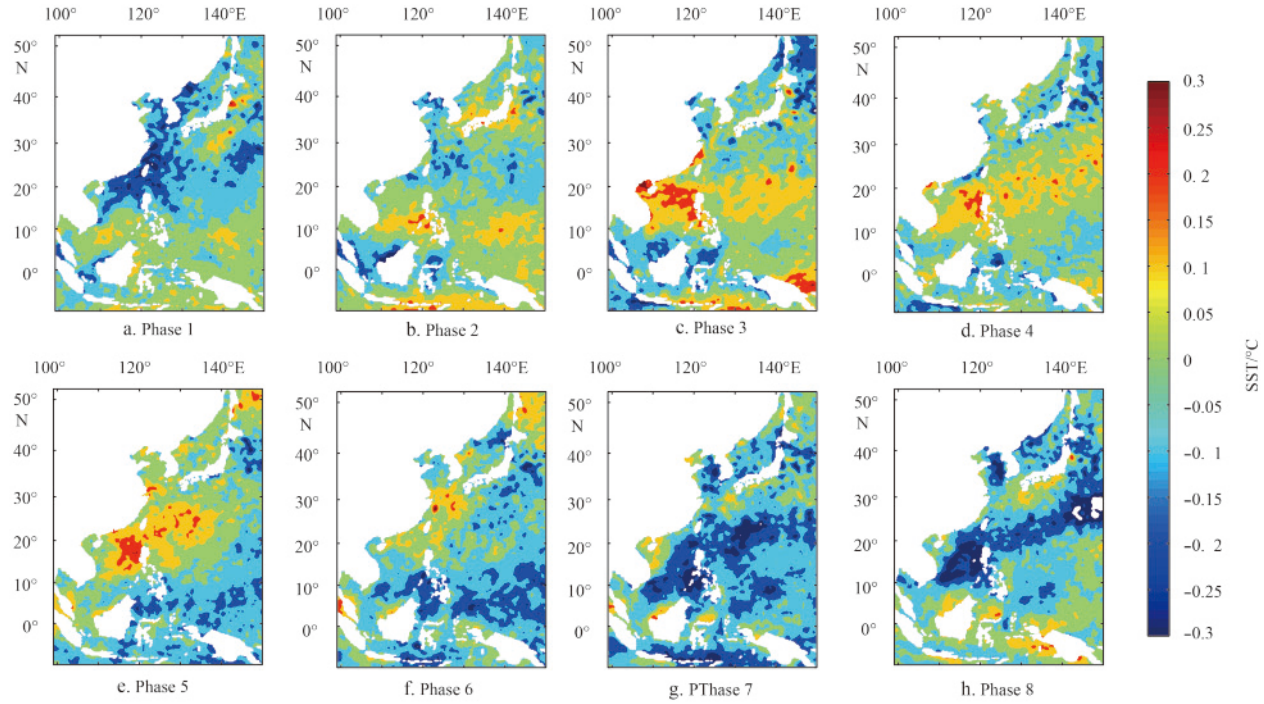

Fig. 6. Composite intraseasonal SST from observations in the 8 MJO phases.

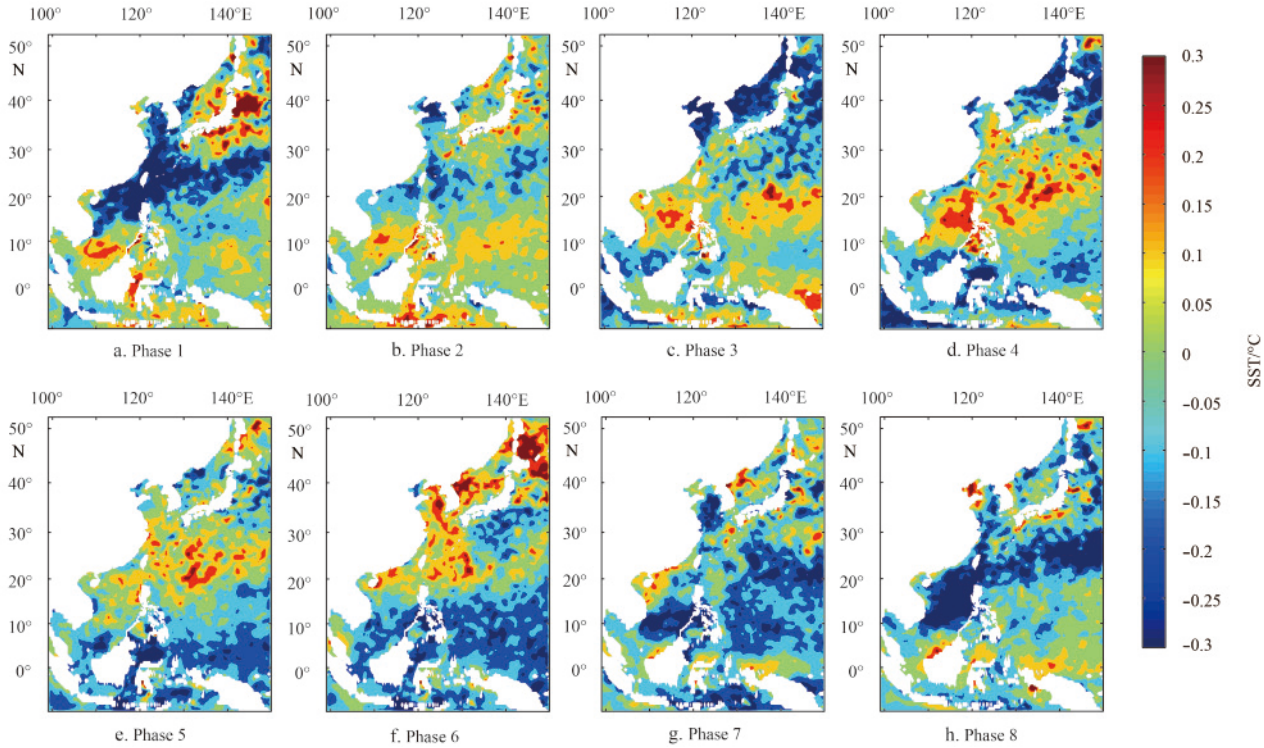

Fig. 7. The same as Fig. 6, but for the intraseasonal SST in CORA.

data. Nevertheless, the depth for the KEO data was only 36 m, which was too shallow for the subsurface variabilities discussed below. Fortunately, four buoys in the INSTANT program were located in the CORA domain. The data were long and deep enough to be compared with the ISVs in CORA and other two reanalysis products. Hence, in the following, we make the intercomparisons between CORA and the other two reanalysis products over the whole CORA domain. In addition, the performance of CORA is qualitatively evaluated with the INSTANT data and the existing knowledge based on limited in situ observations.

The ocean heat content (OHC) in the upper layer, which is defined as the mean ocean temperature in the upper 300 m (Han

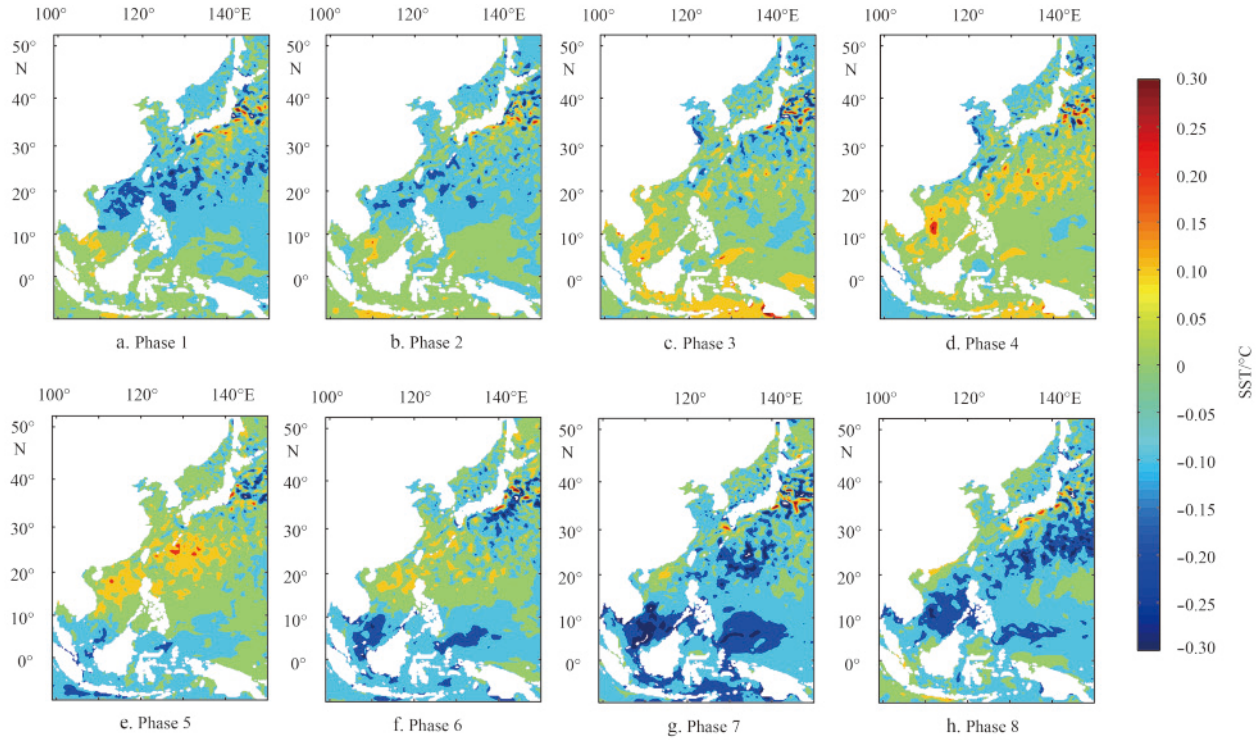

Fig. 8. The same as Fig. 6, but for the intraseasonal SST in ECCO2.

et al., 2013a), is an important variable for the ocean-atmosphere interaction. The intraseasonal OHC is also obtained with the band-pass filter between 20 days and 100 days. The STDs of intraseasonal OHC in CORA, ECCO2, and SODA are shown in Fig. 9. Similar to the situations for SSH and SST, the largest intraseasonal OHC variabilities occur over the Kuroshio extension in all three reanalysis products. CORA has the broadest extent, but ECCO2 has the largest amplitude. Probably due to the coarse spatial resolution, SODA has the smallest ISVs in OHC. Along the Kuroshio, the intraseasonal OHC is moderate in CORA and ECCO2, but is missing in SODA. Besides, the ISVs in OHC is pronounced in ECCO2 in a zonal belt region near the subtropical countercurrent (STCC) around 20°N, but not reproduced in CORA. The ISVs in OHC are probably realistic, since they are likely to be the responses to the westward propagating Rossby waves emanating from the Hawaii islands (Xie et al., 2001). Similar things occur in the northern SCS. The OHC in the northern SCS have obvious ISVs due to the mesoscale eddies moving westward near Luzon strait (Wu and Chiang, 2007), but this is only reproduced in ECCO2. Thus, the ISVs in ECCO2 seems closer to reality and CORA is likely to be unable to resolve such subsurface variabilities.

Similar comparisons are conducted for the ocean currents in the upper layer (Fig. 10), averaged from the surface to 300 m depth. There are four regions with pronounced ISVs in which the distribution is consistent with that of the meso-scale eddies, i.e., the Kuroshio and its extension region, the northern SCS, the western SCS off Vietnam, and the tropical western Pacific region. Pronounced ISVs from the eastern coast of Taiwan to the east coast of Japan along the Kuroshio and the Ryukyu current are obvious in CORA and ECCO2, while the latter is much stronger than the former. However, the ISVs in SODA only occur in the Kurosh-

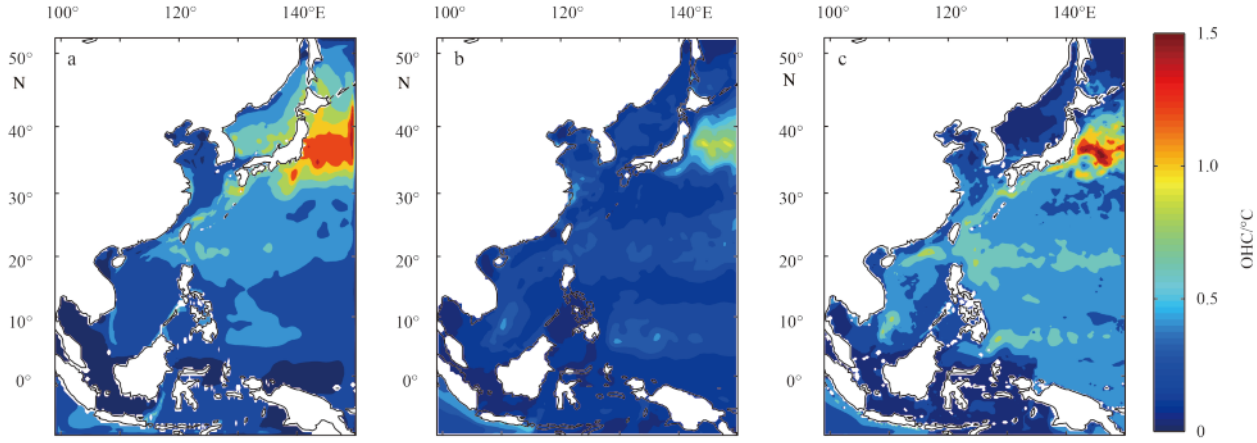

Fig. 9. The standard deviation of the intraseasonal OHC in CORA (a), SODA (b), and ECCO2 (c).

io extension region. Another common feature shared by the three reanalysis products is the large ISVs in ocean currents around the Luzon Strait and over the upwelling region off Vietnam. A notable difference between the dataset resides in the northern SCS. In ECCO2, the ISVs penetrate through the Luzon Strait and extend westward to Hainan Island, which implies that part of Kuroshio Current enters the SCS and spreads over the SCS (Qu et al., 2000; Qu et al., 2006; Wyrtki, 1961). In contrast, in CORA, the high ISVs are blocked at the Luzon Strait without entering the SCS, which is another hypothesis about the relation between Kuroshio and the SCS (Su, 2005; Xu et al., 2003). In SODA, the pattern is similar to that in CORA, but much weaker. In fact, even with *in situ* observations, there are still debates on whether the Kuroshio can efficiently enter the SCS or not. Such discrepancy shows up in different reanalysis products which use different ocean models and different assimilated observations. Of course, a closure of this debate is beyond the scope of this study. There are also strong ISVs in the Pacific bifurcation zone centered around 10°N in ECCO2. Such variabilities are weaker but discernable in SODA. However, they are almost not visible in CORA. Without observations with a high temporal resolution in this region, we are indeed not sure which product is more reliable. Nevertheless, Zhang et al. (2014) reported strong ISVs below 200 m down to about 900 m with mooring observations at 8°N and 127°3′E (located at the red star in Fig. 10), which happened to be in this region. The vertical profiles of intraseasonal meridional velocities at 8°N and 127°E, which is the closest grid point in CORA to the mooring position, are shown in Fig. 11. For SODA and ECCO2, the mean vertical profiles at the four grid points around 8°N and 127°E are also shown in Fig. 11. CORA and ECCO2 show pronounced ISVs above 200 m, which are consistent with Fig. 10. However, only ECCO2 reproduce strong ISVs below 200 m, which is, at least qualitatively, consistent with the mooring observations. The result of the intraseasonal zonal velocities at the same location is similar to that of the meridional velocities (not shown). As shown in Fig. 12a, the buoy deployed in the northern Ombai Strait during the INSTANT program captured pronounced ISVs around 200 m and below 500 m. Around 200 m depth, only ECCO2 reproduces the strong ISVs (Fig. 12d). CORA show weaker ISVs (Fig. 12b) and SODA hardly show any ISVs (Fig. 12c). Below 500 m, the ISVs in ECCO2 and CORA are discernible, but are much weaker than the buoy observations. The situations for the other three INSTANT buoys (one in the southern Ombai Strait and two in the western and the eastern Lombok Strait) are similar to the above (not shown), i.e., ECCO2 yields pronounced ISVs around 200 m which are comparable to the INSTANT data, but the subsurface ISVs in CORA and SODA are much weaker than observations. Therefore, a reasonable hypothesis is that ECCO2 is closer to the reality and CORA misses the ISVs at the subsurface.

5 Discussion and conclusions

Ocean reanalysis products already became a major data source for oceanography. Several global reanalysis products, of which ECCO2 and SODA are two widely-used ones, have been made and been extensively validated. However, due to the limitation of the model resolution and data availability over the China's seas and adjacent regions, mismatches between the global reanalysis and observations are noticeable and lead to big concerns when applying these products in local regions. Therefore, the China Ocean Reanalysis (CORA) – a regional reanalysis product focusing on the China's seas and adjacent regions – was created by the National Marine Data & Information Service. The seasonal and interannual variabilities in CORA were evaluated before. Since there are also pronounced ISVs in the CORA domain, the ability of CORA to reproduce the ISVs is assessed in this study, based on comparisons with observations, as well as ECCO2 and SODA.

CORA successfully reproduces the pattern and amplitude of intraseasonal SSHs in the Kuroshio extension, in the zonal belt centered around 20°N, in the northern SCS, and in the upwelling region off Vietnam. There are huge intraseasonal SSHs in the East China Sea, which are not captured by either products. Considering the possible large errors of altimeter data in the coastal region, such large ISVs in the altimeter data still require confirmations with *in situ* observations. CORA also reproduces the intraseasonal SSTs in the Kuroshio extension and northwestern Pacific reasonably well. The intraseasonal SSTs in East China Sea and Japan Sea are captured, but with a lower amplitude. In CORA, the correlation between the ISVs at the surface and the MJO, as well as the composite ISVs with respect to the MJO phases, are similar to those in reality as a result of assimilating satellite remote sensing SST data. But the correlation coefficients and the composite amplitudes are overestimated in CORA, which

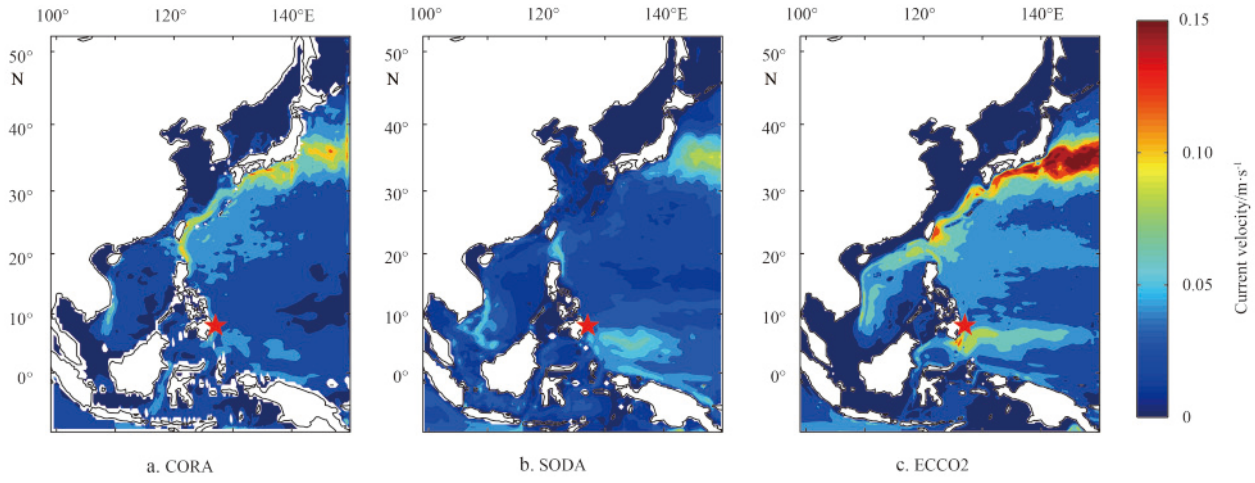

Fig. 10. The same as Fig. 9, but for the intraseasonal vertically-mean ocean current. Red stars denote the mooring location reported in Zhang et al. (2014).

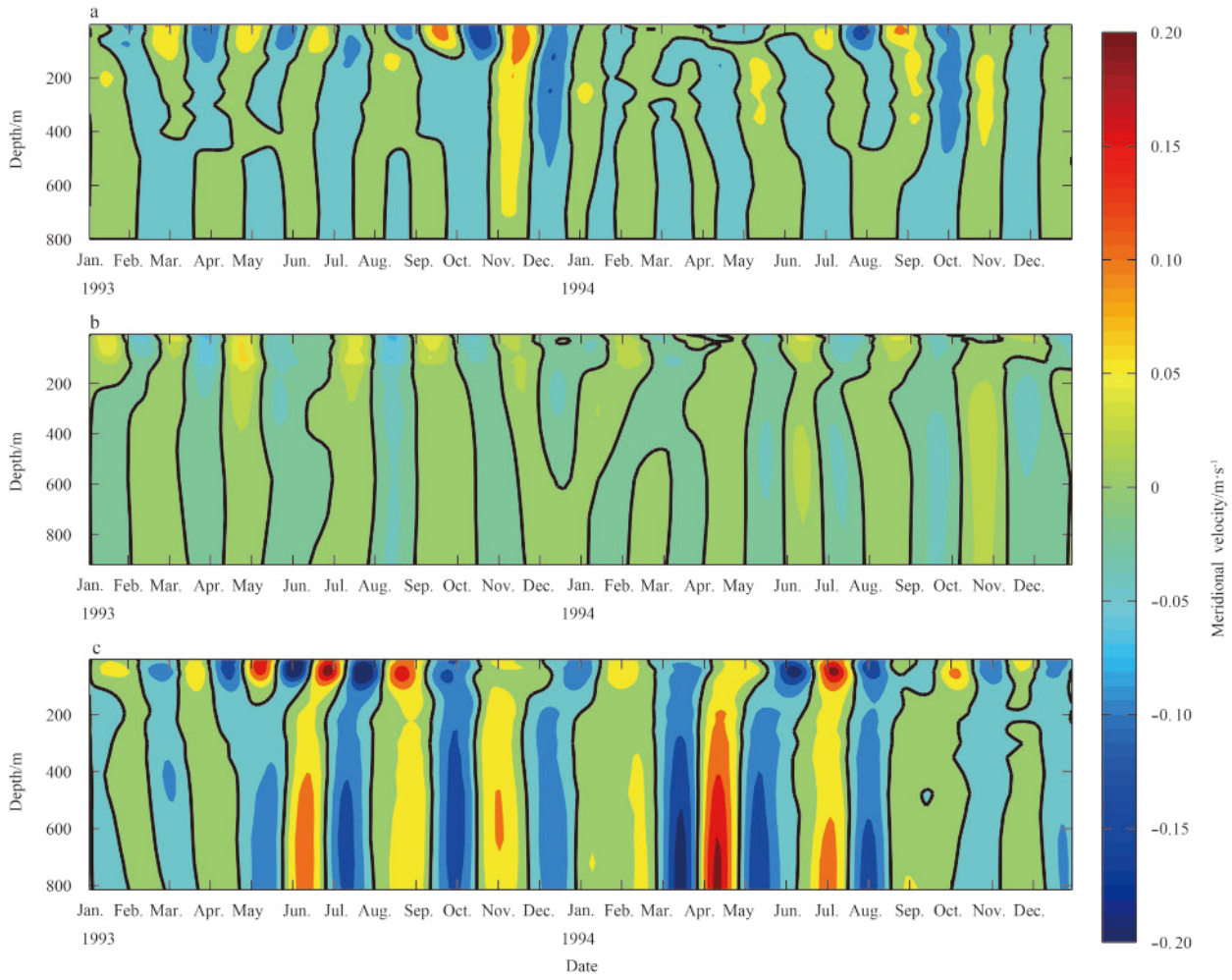

Fig. 11. Vertical profiles of intraseasonal meridional velocities in CORA (a), SODA (b), and ECCO2 (c) for two years. The location is 8°N and 127°E, which is the closest CORA grid point to the mooring location (red stars in Fig. 10). Black contours indicate zero velocities.

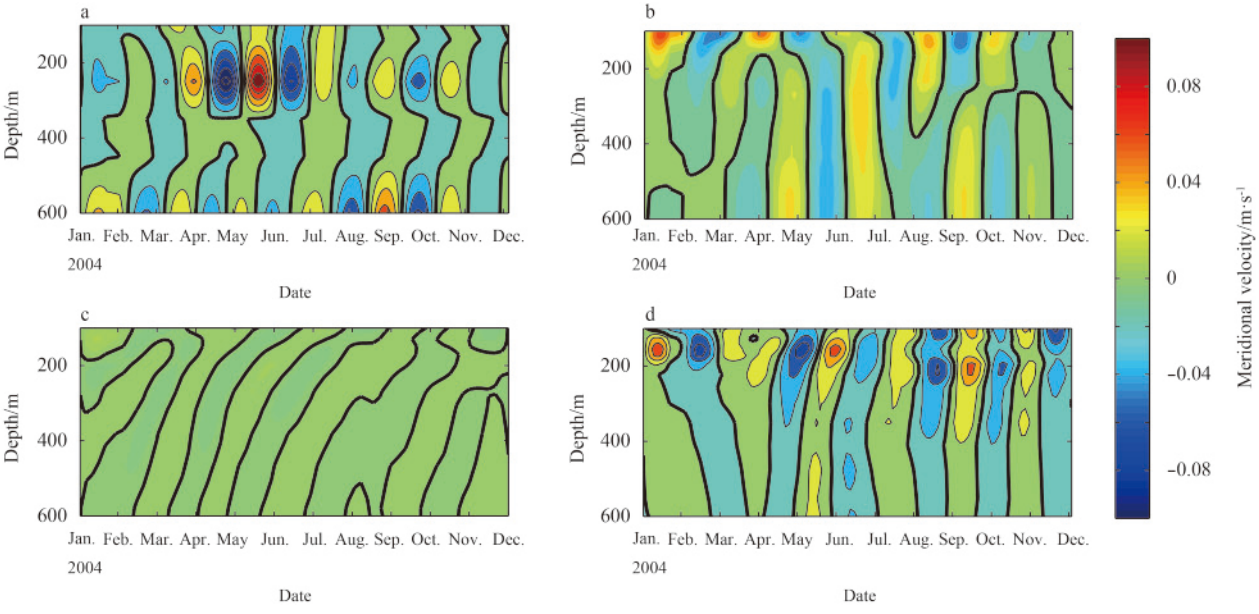

Fig. 12. Vertical profiles of intraseasonal meridional velocities at the northern Ombai Strait (a), CORA (b), SODA (c), and ECCO2 (d) for the year 2004 from January 10 to December 4. Black contours indicate zero velocities.

may be due to the weak diapycnal eddy diffusivity in current model and the lack of ocean-atmospheric coupling. In conclusion, for the ISVs at the ocean surface, CORA has a superior performance to the other two reanalysis products in the CORA domain. Therefore, CORA should be a better choice, compared with ECCO2 and SODA, if one wants to study the ISVs in this region.

For the ISVs in ocean currents and at the subsurface, there are no reliable observations over the whole region. Hence, comparisons can only be done between the three products and some isolated observations. For both OHC and mean ocean current in the upper layer, ECCO2 has the strongest ISVs, CORA follows, and SODA is the weakest. An interesting finding is that the three products endorse two hypotheses on the intrusion of Kuroshio into the SCS, which is still a hot debate now. According to the comparisons with limited in-situ observations, it is likely that the strong ISVs in ECCO2 are closer to reality. If so, it can be concluded that CORA has some abilities to reproduce the pattern of ISVs at the subsurface but the amplitudes require a considerable increase.

In summary, CORA benefits from its high resolution and more observations for assimilation. As a result, it yields satisfactory ISVs at the surface. However, its reproduction of ISVs at the subsurface needs further improvement. Consequently, the suggestion for the application of CORA to the research on oceanic ISVs is straightforward, i.e., CORA is a preferable choice for the processes at the surface, but great cares have to be taken for the subsurface processes.

Acknowledgements

We are grateful to the National Marine Data and Information Service of China who provided the CORA products.

References

Carton J A, Giese B S. 2008. A reanalysis of Ocean climate using Simple Ocean Data Assimilation (SODA). Monthly Weather Review, 136(8): 2999–3017

Carton J A, Chepurin G, Cao Xianhe. 2000a. A simple ocean data assimilation analysis of the global upper ocean 1950–95. Part II: results. Journal of Physical Oceanography, 30(2): 311–326

Carton J A, Chepurin G, Cao Xianhe, et al. 2000b. A simple ocean data assimilation analysis of the global upper ocean 1950–95. Part I: methodology. Journal of Physical Oceanography, 30(2): 294–309

Ezer T, Mellor G L. 2004. A generalized coordinate ocean model and a comparison of the bottom boundary layer dynamics in terrain-following and in z-level grids. Ocean Model, 6(3–4): 379–403

Fofonoff N P, Millard R C. 1983. Algorithms for computation of fundamental properties of seawater. Woods Hole Oceanographic Institution.

Han Guijun, Fu Hongli, Zhang Xuefeng, et al. 2013a. A global ocean reanalysis product in the China Ocean Reanalysis (CORA) project. Advances in Atmospheric Sciences, 30(6): 1621–1631

Han Guijun, Li Wei, Zhang Xuefeng, et al. 2011. A regional Ocean reanalysis system for coastal waters of China and adjacent seas. Advances in Atmospheric Sciences, 28(3): 682–690

Han Guijun, Li Wei, Zhang Xuefeng, et al. 2013b. A new version of regional Ocean reanalysis for coastal waters of China and adjacent seas. Advances in Atmospheric Sciences, 30(4): 974–982

Kajikawa Y, Yasunari T, Wang Bin. 2009. Decadal change in intraseasonal variability over the South China Sea. Geophysical Research Letters, 36(6): L06810

Kobashi F, Kawamura H. 2001. Variation of sea surface height at periods of 65–220 days in the subtropical gyre of the North Pacific. Journal of Geophysical Research, 106(C11): 26817–26831

Li Wei. 2008. Numerical study of the Kuroshio front to the East of Taiwan (in Chinese)[dissertation]. Qingdao: Ocean University of China

Li Wei, Xie Yuanfu, He Zhongjie, et al. 2008. Application of the multigrid data assimilation scheme to the China Seas' temperature forecast. J Atmos Oceanic Tech, 25(11): 2106–2116

Li Yuanlong, Han Weiqing, Shinoda T, et al. 2014. Revisiting the Wintertime Intraseasonal SST Variability in the Tropical South Indian Ocean: Impact of the Ocean Interannual Variation. Journal of Physical Oceanography, 44(7): 1886–1907

Lin Xiaopei, Yin Yuqi, Zhai Ping, et al. 2014. A mechanism for the latitudinal dependence of peak-spectrum sea surface height variability. J Geophys Res, 119(2): 1431–1444, doi: 10.1002/2013JC009642

Madden R A, Julian P R. 1971. Detection of a 40–50 day oscillation in the zonal wind in the tropical Pacific. J Atmos Sci, 28(5): 702–708

Matthews A J, Singhruck P, Heywood K J. 2007. Deep Ocean impact of a Madden-Julian oscillation observed by Argo floats. Science, 318(5857): 1765–1769

Mellor G L, Häkkinen S, Ezer T, et al. 2002. A generalization of a sigma coordinate ocean model and an intercomparison of model vertical grids. In: Pinard N, Woods J, eds. Ocean Forecasting: Conceptual Basis and Applications. Berlin: Springer, 55–72

Menemenlis D, Campin J -M, Heimbach P, et al. 2008. ECCO2: high resolution global ocean and sea ice data synthesis. Mercator Ocean Quarterly Newsletter, 31: 13–21

Ponte R M, Wunsch C, Stammer D. 2007. Spatial mapping of time-variable errors in Jason-1 and TOPEX/Poseidon sea surface height measurements. Journal of Atmospheric and Oceanic Technology, 24(6): 1078–1085

Qiao Fangli, Ezer T, Yuan Yeli. 2004. Zonal distribution features of high frequency planetary waves in the oceans derived from satellite altimeter data. Acta Oceanologica Sinica, 23(1): 91–96

Qu Tangdong, Girton J B, Whitehead J A. 2006. Deepwater overflow through Luzon strait. Journal of Geophysical Research, 111(C1): doi: 10.1029/2005JC003139

Qu Tangdong, Mitsudera H, Yamagata T. 2000. Intrusion of the North Pacific waters into the South China Sea. Journal of Geophysical Research, 105(C3): 6415–6424

Reynolds R W, Smith T M, Liu Chunying, et al. 2007. Daily high-resolution-blended analyses for sea surface temperature. Journal of Climate, 20(22): 5473–5496

Stammer D, Chassignet E. 2000. Ocean state estimation and prediction in support of oceanographic research. Oceanography, 13(2): 51–56

Sprintall J, Wijffels S, Gordon A L, et al. 2004. INSTANT: a new international array to measure the Indonesian throughflow. EOS, 85(39): 369

Su Jilan. 2005. Overview of the South China Sea circulation and its dynamics. HaiyangXuebao (in Chinese), 27(6): 1–8

Wang Guihua, Ling Zheng, Wu Renguang, et al. 2013. Impacts of the Madden–Julian oscillation on the summer South China Sea Ocean circulation and temperature. J Climate, 26(20): 8084–8096

Wheeler M C, Hendon H H. 2004. An all-season real-time multivariate MJO index: development of an index for monitoring and prediction. Monthly Weather Review, 132(8): 1917–1932

Wu C R, Chiang T-L. 2007. Mesoscale eddies in the northern South China Sea. Deep Sea Research Part II: Topical Studies in Oceanography, 54(14–15): 1575–1588

Wu Yang. 2012. Characteristics of seasonal and interannual variability of the thermal structure in the upper South China Sea (in Chinese)[dissertation]. Nanjing: Nanjing University of Information Science & Technology

Wu Yang, Cheng Guosheng, Han Guijun, et al. 2013. Analysis of seasonal and interannual variability of sea surface temperature for China Seas based on CORA dataset. HaiyangXuebao (in Chinese), 35(1): 44–54

Wunsch C, Stammer D. 2003. III: OCEAN CIRCULATION: global ocean data assimilation and geoid measurements. Space Science Reviews, 108(1–2): 147–162

Wyrtki K. 1961. Physical oceanography of the southeast Asian waters. NAGA REPORT Vol 2. La Jolla California: The University of California Scripps Institution of Oceanography

Xie Shangping, Chang C H, Xie Qiang, et al. 2007. Intraseasonal variability in the summer South China Sea: wind jet, cold filament, and recirculations. Journal of Geophysical Research, 112(C10): C10008

Xie Shangping, Liu W T, Liu Qinyu, et al. 2001. Far-reaching effects of the Hawaiian Islands on the Pacific ocean-atmosphere system. Science, 292(5524): 2057–2060

Xie Shangping, Xie Qiang, Wang Dongxiao, et al. 2003. Summer upwelling in the South China Sea and its role in regional climate variations. Journal of Geophysical Research, 108(C8): 3261

Xu Jianping, Chai Fei, Liu Zenghong, et al. 2003. Several significant hydrographic characteristics and their formation mechanism in the South China Sea during the spring and summer of 1998. Acta Oceanologica Sinica, 22(4): 491–502

Yang Qingxuan, Tian Jiwei, Zhao Wei, et al. 2014b. Observations of turbulence on the shelf and slope of northern South China Sea. Deep Sea Research Part I: Oceanographic Research Papers, 87: 43–52

Yang Qingxuan, Zhou Lei, Tian Jiwei, et al. 2014a. The roles of kuroshio intrusion and mesoscale eddy in upper mixing in the northern South China Sea. Journal of Coastal Research, 30(1): 192–198

Zhang C. 2005. Madden-Julian Oscillation. Reviews of Geophysics, 43: 1–36

Zhang Dongxiao, Lee T N, Johns W E, et al. 2001. The kuroshio east of Taiwan: modes of variability and relationship to interior ocean mesoscale eddies. Journal of Physical Oceanography, 31(4): 1054–1074

Zeng Guang'en, Lian Shumin, Cheng Xuhua. 2006. EOF analysis of intra-seasonal variabilities of SST in the East China Sea and Yellow Sea. Advances in Marine Science (in Chinese), 24(2): 146–155

Zhang Linlin, Hu Dunxin, Hu Shijian, et al. 2014. Mindanao Current/Undercurrent measured by a subsurface mooring. Journal of Geophysical Research, 119(6): 3617–3628

Zhai Ping. 2008. The distribution characteristic and mechanism of intraseasonal oscillations in global Oceans (in Chinese) [dissertation]. Qingdao: Ocean University of China

Zhou Faxiu, Ding Jie, Yu Shenyu. 1995. The intraseasonal oscillation of sea surface temperature in the South China Sea. Journal of Ocean University of Qingdao (in Chinese), 25(1): 1–6

Zhou Faxiu, Gao Rongzhen. 2002. Intraseasonal variability of the subsurface temperature observed in the South China Sea (SCS). Chinese Science Bulletin, 47(4): 337–342

Zhou Lei, Murtugudde R. 2010. Influences of Madden–Julian oscillations on the eastern Indian Ocean and the maritime continent. Dynamics of Atmospheres and Oceans, 50(2): 257–274

Zhou Lei, Murtugudde R, Jochum M. 2008. Seasonal influence of Indonesian throughflow in the southwestern Indian Ocean. J Phys Oceanogr, 38(7): 1529–1541